

Classification of Spatio-Temporal Data via Asynchronous Sparse Sampling: Application to Flow Around a Cylinder

Ido Bright*

Guang Lin[†]

J. Nathan Kutz^{‡*}

March 1, 2022

Abstract

We present a novel method for the classification and reconstruction of time dependent, high-dimensional data using sparse measurements, and apply it to the flow around a cylinder. Assuming the data lies near a low dimensional manifold (low-rank dynamics) in space and has periodic time dependency with a sparse number of Fourier modes, we employ compressive sensing for accurately classifying the dynamical regime. We further show that we can reconstruct the full spatio-temporal behavior with these limited measurements, extending previous results of compressive sensing that apply for only a single snapshot of data. The method can be used for building improved reduced-order models and designing sampling/measurement strategies that leverage time asynchrony.

1 Introduction

Data-driven methods, often rooted in new innovations of machine learning [1, 2, 3], are becoming transformative tools in the study of complex dynamical systems [4]. Such methods aim to take advantage of the ubiquitous observation across the physical, engineering and biological sciences that meaningful input/output of macroscopic variables are encoded in low-dimensional patterns of dynamic activity [5, 6, 7, 8, 9, 10, 11]. Reduced-order models (ROMs) capitalize on this observation with the goal of producing real-time computational schemes for modeling complex systems (See the recent edited monograph addressing the state of the art in reduced order methods for computational modeling of complex parametrized systems [12]). Complimenting these efforts are new theoretical efforts using sparsity promoting techniques [13, 14, 15, 16, 17, 18, 19, 20] which exploit this fact in order to deal with the practical constraints of a limited number of sensors for data acquisition in the complex system [21, 22, 23, 24, 25]. Such findings lead us to conjecture that a principled approach to sensing in such complex systems will allow us to probe the latent, low-dimensional structure of dynamic activity relating to the fundamental quantities of interest. A direct implication of such a data-driven modeling strategy is that we can gain traction on prediction, state-estimation and control of the complex system. To this end, we demonstrate that asynchronous sparse measurements in both time and space allows for a robust method, i.e. a spatio-temporal compressive sensing method, for classifying the dynamical behavior of a given system. Once classified, it can be used for

*Department of Applied Mathematics, University of Washington, Seattle, WA. 98195-3925. [‡] (kutz@uw.edu). Questions, comments, or corrections to this document may be directed to that email address.

[†]Department of Mathematics and School of Mechanical Engineering, Purdue University, West Lafayette, IN 47907

full state reconstruction and/or future state prediction of the full spatio-temporal system, extending previous works [21, 22] which only reconstructed single time snapshots of the data.

To demonstrate our methodology, we consider a practical implementation of our technique on time-varying fluid flows that are ubiquitous in modern engineering and in the life sciences. Specifically, we use the asynchronous sparse measurements in time and space on the pressure field around a cylinder to classify the Reynolds number and reconstruct the full pressure field. This problem was previously and successfully considered [21, 22] with the view of only considering spatial compressive sensing. The addition of asynchronous time measurements is the new innovation considered here allowing for a more robust architecture for performing the classification task.

Our method is motivated by bio-inspired engineering design principals [26, 27, 28, 29] whereby birds, bats, insects, and fish routinely harness limited measurements of unsteady fluid phenomena to improve their propulsive efficiency, maximize thrust and lift, and increase maneuverability [30, 31, 32, 33, 34, 35]. Indeed, despite their limited number of computational resources and spatially distributed, noisy sensors, they achieve robust flight dynamics and control despite potentially large perturbations in flight conditions (e.g. wind gusts, bodily harm). Such observations suggest the existence of low-dimensional structures in the flow-field that are sparsely sampled and which are exploited for robust control purposes.

The primary innovation here revolves around the compressive sensing ideology. Compressed sensing allows the reconstruction of a signal using a small number of measurements, based on the fact that the signal has a sparse representation in an appropriate basis [13, 14, 15, 16, 17, 18, 19]. This allows the use of less measurements than the Nyquist-Shannon criterion requires [36, 37]. Although typical applications are found in areas spanning signal processing to computer vision, our objective is to use the methodology for the numerical solution of partial differential equations (PDE) and/or direct observations of complex systems. We present a specific example - the incompressible Navier-Stokes flow around a cylinder. However, the framework presented can be applied to a much broader set of equations. At the method's core is the fact that most complex systems, including the flow around a cylinder, exhibit an underlying low-dimensional structure in their dynamics, such an assumption is at the heart of the ROM methodology. Unlike the standard application of compressive sensing for image processing, for example, where the sparse (wavelet) basis is already known, the optimal sparse basis considered here is computed directly from PDE simulations (e.g. through a proper orthogonal decomposition, for instance). Previously, the method was developed to classify the Reynolds number for flow around a cylinder given a single snapshot measurement [21]. However, by using asynchronous temporal measurements as well, the method can be greatly improved. Thus a spatio-temporal version of the compressive sensing architecture is developed and advocated here as the primary result.

The paper is outlined as follows: In Sec. 2 we outline the underlying methods used for the spatio-temporal dimensionality reductions, highlighting how low-rank structures in both space and time are equally exploited. Section 3 outlines the method used for reconstruction of the solution given a sparse set of measurements. Classification of the dynamical regime of the system, which is based upon libraries of dynamical modes, is demonstrated in Sec. 4. Sections 2-4 in combination form the core innovation of this manuscript, leading to the example problem of flow around a cylinder of Sec. 5. A brief conclusion and outlook are given in Sec. 6.

2 Dimensionality Reduction for Data Snapshots

Dimensionality reduction has a long history in regard to theoretical methods applied to complex dynamical systems. Before the advent of computers, dimensionality reduction often was achieved through asymptotic reductions of the governing equations. Indeed, many well characterized theoretical examples of fluid dynamics are due to perturbative reductions of the full system in some parameter regime, e.g. the low Reynolds number limit. Such reductions allow for a simplified model where known analytic methods can be applied to great effect. These asymptotic techniques also serve as the backbone for normal form reductions for characterizing the low-dimensional embedding subspaces where bifurcations in complex systems occur. With the advent of the computer and modern high-performance computing, these same kind of reductions can be achieved through principled approaches such as the proper orthogonal decomposition [38], which is also known with minor variation as Principal Component Analysis (PCA) [39], the Karhunen–Loève (KL) decomposition, the Hotelling transform [40, 41] and/or Empirical Orthogonal Functions (EOFs) [42]. These methods identify the low-dimensional subspaces and modal basis that optimally represent, in an ℓ_2 sense, the dynamics of the system, thus forming the basis of the ROM architecture [12].

For our purposes, consider data that comes from a dynamical system of a single spatial variable x of the form

$$(1) \quad u_t = N(\nu, x, t, u, u_x, u_{xx}, \dots),$$

where $N(\cdot)$ determines the evolution of the complex system which can be a function of space ($x \in [-L, L]$), time ($t \in [0, T]$) and linear and nonlinear terms involving $u(x, t)$ and its derivatives. Additionally, the parameter ν is a bifurcation parameter that determines the dynamical regime of the system. Such systems are typically solved using a numerical discretization scheme where the k th time point ($k = 1, 2, \dots, m$) is given by

$$(2) \quad \mathbf{u}(x, t_k) \rightarrow \mathbf{u}_k = [u(x_1, t_k) \ u(x_2, t_k) \ \dots \ u(x_n, t_k)]^T$$

with the discretization grid $\Delta x = x_{j+1} - x_j \ll 1$, $x_1 = -L$, $x_n = L$ and $n \gg 1$. Thus in a simulation, one has access to all the data in a discretized form in space and time. Moreover the data is high-dimensional since a fine grid (of size n) is typically required for accurate solutions of the partial differential equation.

For various values of the bifurcation parameter ν we assume we have access to the data, either from computation or from dense measurements in time and space. We can arrange the full data into a matrix whose columns are the full discretized state of the system, or snapshots, sampled evenly in time

$$(3) \quad \mathbf{A}_D^\nu = [\mathbf{u}_1 \ \mathbf{u}_2 \ \dots \ \mathbf{u}_m]$$

where $\mathbf{A}_D^\nu \in \mathbb{R}^{n \times m}$. In the application we wish to consider in this manuscript, we assume that we have access only to a subset of the data, based on the position in the spatial grid x_j , i.e. we have a limited number of spatial sensors available that are fixed to a specific spatial location. To be more precise, consider the the projection matrix \mathbf{P}_k whose k nonzero entries determine the spatial locations for data sensors (let $k = 3$ for illustrative purposes):

$$(4) \quad \mathbf{P}_3 = \begin{bmatrix} 1 & 0 & \dots & & & & \dots & 0 \\ 0 & \dots & 0 & 1 & 0 & \dots & & \dots & 0 \\ 0 & \dots & & & \dots & 0 & 1 & 0 & \dots & 0 \end{bmatrix}$$

This example maps out the full state of the system onto 3 measurement locations

$$(5) \quad \tilde{\mathbf{u}} = \mathbf{P}_3 \mathbf{u}.$$

More generally for k measurement locations, we can construct the data matrix

$$(6) \quad \mathbf{A}_S^\nu = [\tilde{\mathbf{u}}_1 \ \tilde{\mathbf{u}}_2 \ \cdots \ \tilde{\mathbf{u}}_m]$$

where $\mathbf{A}_S^\nu \in \mathbb{R}^{k \times m}$. Thus \mathbf{A}_S^ν is a subset of data generated from a small number sensors k where $k \ll n$. Our hypothesis is that the data satisfies the following conditions:

H1 The data in \mathbf{A}_S^ν has a low dimensional representation in the phase space, namely, it can be approximated by a low dimensional vector space while maintaining most of the energy (variance) in the ℓ_2 sense.

To extract the low-rank representation of the data, we apply a singular value decomposition (SVD) to the data matrix to obtain

$$(7) \quad \mathbf{A}_S^\nu = \mathbf{V}_S^\nu \mathbf{\Sigma}_S^\nu \mathbf{U}_S^\nu.$$

The SVD decomposition can be used for producing a principled low-dimensional representation of the data. Truncation is typically achieved by inspection of the diagonal singular value matrix $\mathbf{\Sigma}_S^\nu$. Specifically, d^ν modes are selected that, for instance, represent 99% of the total variance in the data. For data with noise, recent work by Gavish and Donoho [43] provides a principled truncation algorithm to account for the effects of noise.

In our analysis, we reduce the data to d^ν -dimensions for a variety of dynamical regimes ν . This allows us to obtain the approximation to the data matrix

$$(8) \quad \bar{\mathbf{A}}_S^\nu = \bar{\mathbf{V}}_S^\nu \bar{\mathbf{\Sigma}}_S^\nu \bar{\mathbf{U}}_S^\nu,$$

where the barred matrices are d^ν -rank approximations to their unbarred counterparts, ultimately providing the approximation to the full data

$$(9) \quad \mathbf{A}_S^\nu \approx \bar{\mathbf{A}}_S^\nu = \sum_{i=1}^{d^\nu} \sigma_i \mathbf{v}_i^\nu \mathbf{u}_i^\nu.$$

where $\bar{\mathbf{V}}_S^\nu = [\mathbf{v}_1^\nu, \dots, \mathbf{v}_{d^\nu}^\nu]$, $\bar{\mathbf{U}}_S^\nu = [\mathbf{u}_1^\nu \ \mathbf{u}_2^\nu \ \dots \ \mathbf{u}_{d^\nu}^\nu]$, and σ_i are the corresponding diagonal elements $\bar{\mathbf{\Sigma}}_S^\nu$.

In addition to our assumption that (1) exhibits low-dimensional dynamics, there is a large subclass of dynamical systems that also exhibit time dynamics that are nearly periodic. More precisely, in the application considered here, the time dynamics can be approximated by a small number of Fourier modes, thus allowing for a second sparsification step. This leads to the second hypothesis of the current work:

H2 Each row of the matrix $\bar{\mathbf{U}}_S^\nu$ can be approximated, in the ℓ_2 sense, by a small number of Fourier modes in time, namely by cosines and sines.

Given this second hypothesis, our goal now is to further approximate the full data matrix \mathbf{A}_S^ν by a sparse number of Fourier modes. Thus in the modal decomposition (7), the matrix containing the time dynamic modes \mathbf{u}_k^ν is approximated by

$$(10) \quad \mathbf{u}_i^\nu = \sum_{j=1}^{n_i^\nu} (a_{i,j}^{c,\nu} \mathbf{c}_{i,j}^\nu + a_{i,j}^{s,\nu} \mathbf{s}_{i,j}^\nu),$$

where n_i^ν is the small (sparse) number of Fourier modes retained with

$$\mathbf{c}_{i,j}^\nu = [\cos(\omega_{i,j}^\nu t_1), \cos(\omega_{i,j}^\nu t_2), \dots, \cos(\omega_{i,j}^\nu t_N)] \quad (11a)$$

$$\mathbf{s}_{i,j}^\nu = [\sin(\omega_{i,j}^\nu t_1), \sin(\omega_{i,j}^\nu t_2), \dots, \sin(\omega_{i,j}^\nu t_N)] \quad (11b)$$

and where $\omega_{i,j}^\nu$ is the angular frequency obtained by the Fourier transform.

The low-rank approximation by the SVD (9) and the sparse Fourier mode approximation (10) can be combined to give the time-space reduction

$$(12) \quad \mathbf{A}_S^\nu = \sum_{i=1}^{d^\nu} \sigma_i \mathbf{v}_i \sum_{j=1}^{n_i^\nu} (a_{i,j}^{c,\nu} \mathbf{c}_{i,j}^\nu + a_{i,j}^{s,\nu} \mathbf{s}_{i,j}^\nu) = \sum_{i=1}^{d^\nu} \sum_{j=1}^{n_i^\nu} (\alpha_{i,j}^{c,\nu} \mathbf{v}_i \mathbf{c}_{i,j}^\nu + \alpha_{i,j}^{s,\nu} \mathbf{v}_i \mathbf{s}_{i,j}^\nu),$$

where $\alpha_{i,j}^{c,\nu} = \sigma_i a_{i,j}^{c,\nu}$ and $\alpha_{i,j}^{s,\nu} = \sigma_i a_{i,j}^{s,\nu}$.

We now perform the final dimensionality-reduction step in our analysis. Specifically, we define $(\alpha_{i,j}^\nu)^2 = (\alpha_{i,j}^{s,\nu})^2 + (\alpha_{i,j}^{c,\nu})^2$ and choose m^ν of the largest $\alpha_{i,j}^\nu$ so that their sum of squares approximates the energy up to a given threshold for truncation. This allows us to obtain the final low-rank approximation of the data matrix

$$(13) \quad \mathbf{A}_S^\nu \approx \sum_{k=1}^{m^\nu} (\alpha_k^{c,\nu} \mathbf{v}_{i_k}^\nu \mathbf{c}_{i_k,j_k}^\nu + \alpha_k^{s,\nu} \mathbf{v}_{i_k}^\nu \mathbf{s}_{i_k,j_k}^\nu).$$

Note that we do not need to store the complete vectors \mathbf{c}_{i_k,j_k}^ν and \mathbf{s}_{i_k,j_k}^ν , but only the vectors $\mathbf{v}_{i_k}^\nu$, and the frequencies ω_{i_k,j_k}^ν obtained by the Fast Fourier Transform. Approximation (13) allows us to use a small number of measurements in time and space to reconstruct an approximation to the entire data matrix. This is the primary innovation of this work.

3 Reconstruction from Sparse Measurements

The primary objective in this work is to use sparse measurements in space and time to reconstruct the full state \mathbf{u} of (1) and (2). To this end, consider that we are given m^ν measurements

$$(14) \quad \mathbf{p} = [\mathbf{p}_1 \ \mathbf{p}_2 \ \dots \ \mathbf{p}_{m^\nu}]$$

at the space-time points

$$(15) \quad (t_i, x_i) = (\tau_i, \chi_i) \quad \text{for } i = 1, 2, \dots, m^\nu.$$

Recall that we assumed that the measurements can be respresented sparsely by the parameter ν in (13), namely:

$$(16) \quad \mathbf{p}_i = \sum_{k=1}^{m^\nu} [\mathbf{v}_{i_k}^\nu]_{\chi_i} (\cos(\omega_{i_k,j_k}^\nu (\tau_i + \phi)) + \sin(\omega_{i_k,j_k}^\nu (\tau_i + \phi))),$$

where $[\mathbf{v}]_l$ denotes the l 'th element of the vector, and ϕ is an unknown phase.

We relax this representation by folding in the unknown phase into additional amplitude parameters. The new representation takes the form

$$(17) \quad \mathbf{p}_i = \sum_{k=1}^{m^\nu} [\mathbf{v}_{i_k}^\nu]_{\chi_i} (A_{i_k, j_k}^\nu \cos(\omega_{i_k, j_k}^\nu \tau_i) + B_{i_k, j_k}^\nu \sin(\omega_{i_k, j_k}^\nu \tau_i)).$$

Note that for each ω_{i_k, j_k}^ν , there are distinct A_{i_k, j_k}^ν and B_{i_k, j_k}^ν that do not depend on i . Thus there are a total of $2m^\nu$ amplitude parameters that need to be determined.

The representation (17) is for a single measurement. The total number of measurements m^ν , as given by (14), can be represented in matrix form by

$$(18) \quad \mathbf{p} = \Phi^\nu \mathbf{b},$$

where the odd and even columns of Φ^ν are $[\Phi^\nu]_{i, 2j-1} = [\mathbf{v}_{i_k}^\nu]_{\chi_i} \cos(\omega_{i_j, j_j}^\nu \tau_i)$ and $[\Phi^\nu]_{i, 2j} = [\mathbf{v}_{i_k}^\nu]_{\chi_i} \sin(\omega_{i_j, j_j}^\nu \tau_i)$ so that

$$(19) \quad \Phi^\nu = \begin{bmatrix} [\mathbf{v}_{i_1}]_{\chi_1} \cos(\omega_{i_1, j_1}^\nu \tau_1) & [\mathbf{v}_{i_1}]_{\chi_1} \sin(\omega_{i_1, j_1}^\nu \tau_1) & \cdots & [\mathbf{v}_{i_{m^\nu}}]_{\chi_1} \sin(\omega_{i_{m^\nu}, j_{m^\nu}}^\nu \tau_1) \\ [\mathbf{v}_{i_1}]_{\chi_2} \cos(\omega_{i_1, j_1}^\nu \tau_2) & [\mathbf{v}_{i_1}]_{\chi_2} \sin(\omega_{i_1, j_1}^\nu \tau_2) & \cdots & [\mathbf{v}_{i_{m^\nu}}]_{\chi_2} \sin(\omega_{i_{m^\nu}, j_{m^\nu}}^\nu \tau_2) \\ \vdots & \vdots & \ddots & \vdots \\ [\mathbf{v}_{i_1}]_{\chi_N} \cos(\omega_{i_1, j_1}^\nu \tau_N) & [\mathbf{v}_{i_1}]_{\chi_N} \sin(\omega_{i_1, j_1}^\nu \tau_N) & \cdots & [\mathbf{v}_{i_{m^\nu}}]_{\chi_N} \sin(\omega_{i_{m^\nu}, j_{m^\nu}}^\nu \tau_N) \end{bmatrix}$$

with

$$(20) \quad \mathbf{b} = \begin{bmatrix} A_{i_1, j_1}^\nu \\ B_{i_1, j_1}^\nu \\ A_{i_2, j_2}^\nu \\ B_{i_2, j_2}^\nu \\ \vdots \\ B_{i_{m^\nu}, j_{m^\nu}}^\nu \end{bmatrix}.$$

Note that the matrix Φ^ν depends on the time-space locations where measurements are made. The reconstruction based upon (13) can then be accomplished using a standard Moore-Penrose pseudo-inverse [44] given the measurements \mathbf{p} . This allows for computing the unknowns \mathbf{b} and performing the full state reconstruction with limited measurements.

4 Dynamical Libraries and Classification

The previous section considered our ability to perform a reconstruction or approximation of the full state of the system using a limited number of measurements. The reconstruction was for a specific value of the bifurcation parameter ν . However, there may be many different dynamical regimes of (1) that are of interest and have low-dimensional dynamics [21, 22]. For each dynamical regime ν_j , we can then construct the measurement matrices $\Phi^{\nu_1}, \dots, \Phi^{\nu_M}$ where we assume there are M dynamical regimes of interest $(\nu_1, \nu_2, \dots, \nu_M)$. We can collect these various measurement matrices into a single library matrix:

$$(21) \quad \Psi = [\Phi^{\nu_1} \ \Phi^{\nu_2} \ \dots \ \Phi^{\nu_M}].$$

Thus Ψ contains all the low-rank approximations for space-time measurements from the M dynamical regimes. Such a database building strategy is also at the forefront of ROM architectures since ROMs are neither robust with respect to parameter changes nor cheap to generate. Thus methods based on a database of ROMs coupled with a suitable interpolation schemes greatly reduces the computational cost for aeroelastic predictions while retaining good accuracy [12, 45].

Our objective ultimately is to use a small number of measurements to reconstruct the full state of the system. However, in order to do so efficiently and effectively, one needs to classify which dynamical regime ν_j the system is in so that the correct Φ^{ν_j} can be used for the reconstruction. The classification is predicated on the idea that our measurement locations (14) have the sparsest reconstruction (of the form (17)), given the correct parameter ν_j [21, 22]. To employ this fact in a classification algorithm, we shall represent the point \mathbf{p}_i using all the possible parameters μ_j , generate an underdetermined system, and use a compressive sensing algorithm to obtain the sparsest representation. Our hypothesis is that the non-zero coefficients A_{i_k, j_k}^ν and B_{i_k, j_k}^ν will be concentrated in the correct ν . Specifically we shall construct an underdetermined linear system and solve it using a sparsity promoting algorithm in order to identify the correct μ_j . Thus classification is based upon ℓ_1 optimization whereas reconstruction relies on an ℓ_2 projection unto the correctly identified basis.

To be more precise, our classification is based on the following minimization problem

$$(22) \quad \min \|\mathbf{a}\|_1 \text{ s.t. } \mathbf{p} = \Psi \mathbf{a}$$

where the unknown vector \mathbf{a} determines the weighting of the library elements Ψ unto the measurement \mathbf{p} . The ℓ_1 minimization is a sparsity promoting algorithm that attempts to give a solution \mathbf{a} that has as many zeros as possible. The non-zero components are used as an indicator for the dynamical regime and modes, ν_j and Φ^{ν_j} respectively. Here, however, the classification exploits both time and space measurements, whereas previous work [21, 22] only considered measurements at a single fixed time for classification.

Classification can be accomplished by considering a relaxed form of the minimization by a LASSO algorithm [46]

$$(23) \quad \min \|\mathbf{a}\|_1 \text{ s.t. } \|\mathbf{p} - \Psi \mathbf{a}\|_2 < \delta,$$

for some parameter δ . This minimization problem minimizes the error, in an ℓ_2 sense, between the measurements and the projection on to the library with the sparsest vector \mathbf{a} . The sparse solution \mathbf{a} can then be used to determine the dynamical regime ν_j the system is in. Once determined, reconstruction can be achieved via (17). Specifically, the classification of the dynamical regime is done by summing the absolute value of the coefficients of \mathbf{a} that corresponds to each dynamical regime ν_j . To account for regimes with a larger number of coefficients allocated for their dynamical regime, we normalize by dividing by the square root of the number of POD modes allocated in \mathbf{a} for each μ_j . The classified regime μ_j is the one that has the largest magnitude after execution of this algorithm.

5 Application: Flow Around a Cylinder

We demonstrate the sparse time-space sampling algorithm developed on a canonical problem of applied mathematics: the flow around a cylinder. This problem is well understood and has already been the subject of studies concerning sparse spatial measurements [21, 23, 47, 48]. Specifically, it

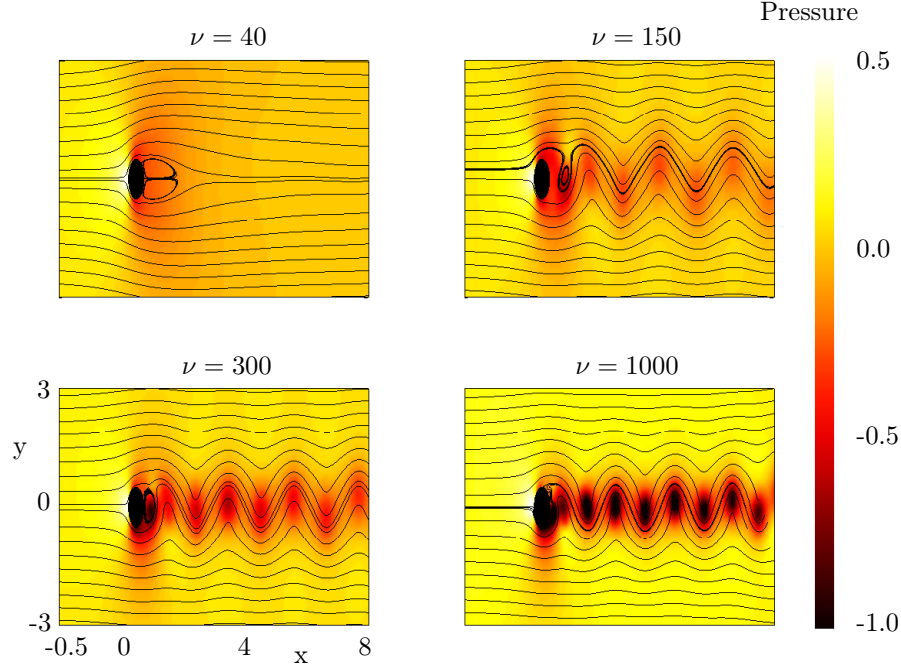


Figure 1: Stream lines and pressure field near the cylinder for a typical snapshot taken for Reynolds numbers (a) $\nu = 40$, (b) $\nu = 150$, (c) $\nu = 300$, and (d) $\nu = 1000$.

is known that for low to moderate Reynolds numbers, the dynamics is spatially low-dimensional and POD approaches have been successful in quantifying the dynamics [23, 49, 50, 51, 52]. Additionally, the time dynamics is nearly periodic, thus suggesting that the asynchronous sampling in time advocated here can be exploited for this problem. The Reynolds number plays the role of the bifurcation parameter ν in (1).

The data we consider comes from numerical simulations of the incompressible Navier-Stokes equation:

$$\frac{\partial u}{\partial t} + u \cdot \nabla u + \nabla p - \nu \nabla^2 u = 0 \quad (24a)$$

$$\nabla \cdot u = 0 \quad (24b)$$

where $u(x, y, t) \in \mathbb{R}^2$ represents the 2D velocity, and $p(x, y, t) \in \mathbb{R}$ the corresponding pressure field. The boundary conditions are as follows: (i) Constant flow of $u = (1, 0)^T$ at $x = -15$, i.e., the entry of the channel, (ii) Constant pressure of $p = 0$ at $x = 25$, i.e., the end of the channel, and (iii) Neumann boundary conditions, i.e. $\frac{\partial u}{\partial \mathbf{n}} = 0$ on the boundary of the channel and the cylinder (centered at $(x, y) = (0, 0)$ and of radius unity).

5.1 The Data: Snapshots of Fluid Pressure

Our data comes from numerical simulation of the incompressible Navier-Stokes equation (24), computed using the Nektar++ package [53], which produces accurate results using a high-order finite element method. The algorithm uses a non-uniform mesh consisting of 228 grid-points, with the

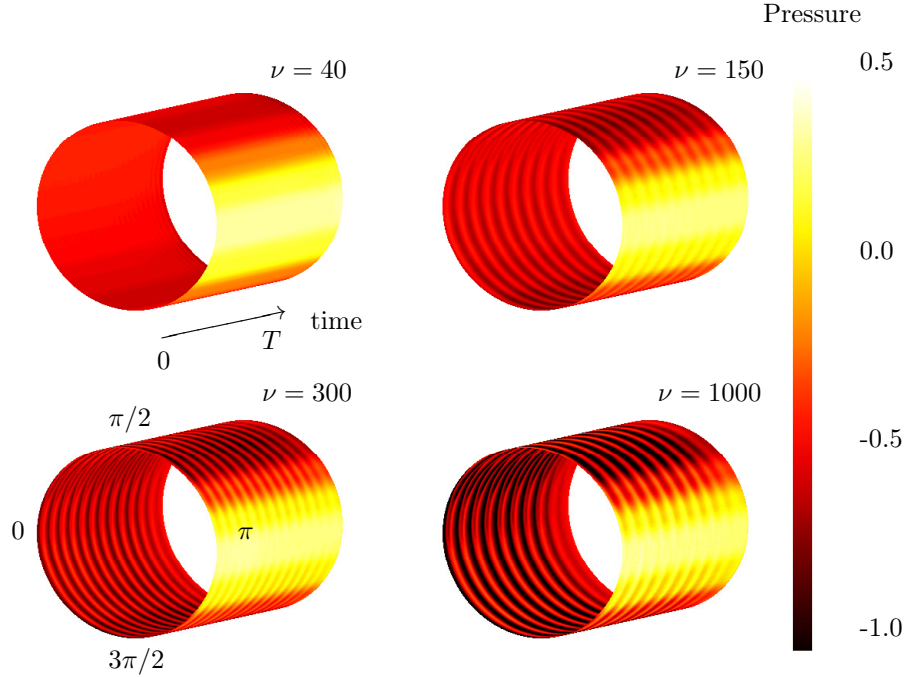


Figure 2: Time evolution of the pressure field around the cylinder for increasing Reynolds numbers $\nu = 40$ ($T = 8$), $\nu = 150$ ($T = 8$), $\nu = 300$ ($T = 20$), and $\nu = 1000$ ($T = 20$).

high-order method producing 66,000 Gaussian quadrature points, i.e. the numerical discretization yields an $n = 66,000$ dimensional system. Figure 1 shows typical snapshots of the streamlines and pressure profiles taken once the system transients have died away and the flow has reached equilibrium or a time-periodic state for various Reynolds numbers.

The different dynamical regimes of (24) correspond to different Reynolds number flow. Thus the classification and reconstruction problem we consider involves library elements extracted from the flow at Reynolds numbers $\nu = 40, 150, 300, 800, 1000$. Specifically, our measurements are based on the pressure field at the perimeter of the cylinder where sensors could be easily placed. In particular, a sparse number of such sensors are used to classify (identify) the Reynolds number and reconstruct the pressure field around the cylinder and in the fluid flow. Note that placing sensors in the fluid flow itself may be valid for lab experiments and computer simulations. However no realistic system of interest, such as an airfoil or insect wing, places sensors directly in the flow field behind the structure. Thus there is a clear reliance on limited measurements on the cylinder itself.

The time evolution of the pressure field on the perimeter of the cylinder is shown in Figure 2 for several Reynolds numbers. As can be seen, increasing the Reynolds number drives the dynamics from a steady-state configuration to a time-periodic evolution. The waterfall plots of the pressure dynamics on the cylinder are essentially the snapshots used for projecting the dynamics onto a low-dimensional manifold through the SVD, i.e. the snapshots provide the data necessary for the low-rank, POD methodology [38].

For each relevant value of the parameter ν we perform an SVD on the data matrix in order to apply the dimensionality reduction method described in Sec. 2. It is well known that for relatively

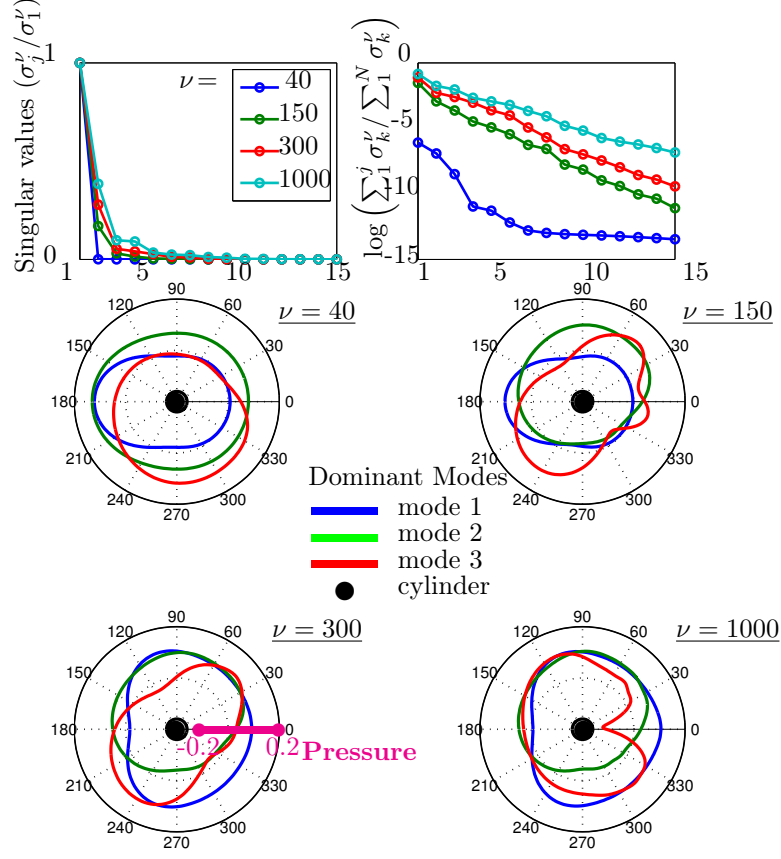


Figure 3: Normalized decay of singular values (top left) of the data matrix for various Reynolds number $\nu = 40, 150, 300, 1000$ (top right on logarithmic scale). As the Reynolds number increases, a higher dimensional space is needed to preserve the same amount of energy. The dominant three pressure modes are shown in polar coordinates. The pressure scale is in magenta (bottom left).

low Reynolds number, a fast decay of the singular values is observed. This can be seen in Fig. 3 along with the 3 most dominant POD modes. Thus for every Reynolds number $\nu = 40, 150, 300, 800, 1000$, we apply the procedures described in Sec. 2 and 3 on the data matrix \mathbf{A}^ν in order to compute the quantities $\mathbf{v}_{i_k}^\nu$ and ω_{i_k, j_k}^ν .

5.2 Sparse Representation

For every Reynolds number we keep 99% of the total energy (variance) which gives for the Reynolds numbers $\nu = 40, 150, 300, 800, 1000$ considered a total of 1, 3, 3, 9, 9 POD modes to represent the dynamics. More precisely, it determines the number of non-zero coefficients (1, 3, 3, 9, 9) in the sparse approximation (13) (i.e. non zero $\alpha_k^{c, \nu}$'s and $\alpha_k^{s, \nu}$'s). The specific modes chosen by our representation, based on the singular value analysis, namely on the magnitude of $(\alpha_{i,j}^\nu)^2 = (\alpha_{i,j}^{c, \nu})^2 +$

Table 1: Sparse Representation: The table contains the top 3 coefficients in the expansion (13), where we specify $(\alpha_{i,j}^\nu)^2 = (\alpha_{i,j}^{c,\nu})^2 + (\alpha_{i,j}^{s,\nu})^2$

Reynolds Number	# Modes	Top 3 Coefficients		
$\nu = 40$	1	$\alpha_{1,0}^{40} = 1$		
$\nu = 150$	3	$\alpha_{1,0}^{150} = 0.97$	$\alpha_{2,T=170}^{150} = 0.03$	
$\nu = 300$	3	$\alpha_{1,0}^{300} = 0.92$	$\alpha_{2,T=375}^{300} = 0.07$	
$\nu = 800$	9	$\alpha_{1,0}^{800} = 0.87$	$\alpha_{2,T=343}^{800} = 0.11$	$\alpha_{3,T=172}^{800} = 0.04$
$\nu = 1000$	9	$\alpha_{1,0}^{1000} = 0.85$	$\alpha_{2,T=333}^{1000} = 0.12$	$\alpha_{3,T=166}^{1000} = 0.06$

Table 2: The error rate of our algorithm with noise that is normally distributed with the standard deviation increasing across the columns. It can be seen that for low to no additive error choosing a small parameter δ for the Lasso 23 provides a good performance, while once the error is increased then the algorithm fails, and provides result that are not any better than guessing. Note that increasing the Lasso parameter δ provides improved performance for higher error, while decreasing the performance for low or no error.

Error (std)	0	2^{-7}	2^{-5}	2^{-4}
$\delta = 0.1$	0.89	0.88	0.2	0.2
$\delta = 0.7$	0.8	0.82	0.83	0.82

$(\alpha_{i,j}^{s,\nu})^2$ is found in Table 1.

5.3 Results

We applied the sparse classification algorithm in Sec. 4 to the training data collected in the previous subsection. Based on previous results [21], we have chosen the sparse measurements at positions corresponding to maxima and minima points of the dominant spatial modes (the \mathbf{v}_i''). Specifically 20 such position where chosen. The classification algorithm was applied to 100 measurements randomly selected over the time interval of training. Namely, classification was based on 2.5% of the data. The results of classification subject to noise with a random distribution is presented in Table 2.

It should be noted once again that the method demonstrated here extends previous work [21, 22] by considering the full spatio-temporal dynamics. Specifically, previous findings were associated with successfully classifying and reconstructing a single snapshot in time. Here, the much more difficult task is considered of reconstruction the entire spatio-temporal behavior with limited measurements. The results presented show the method is quite effective in this task, thus providing a potentially transformational paradigm for taking advantage of limited measurements of a complex, spatio-temporal system.

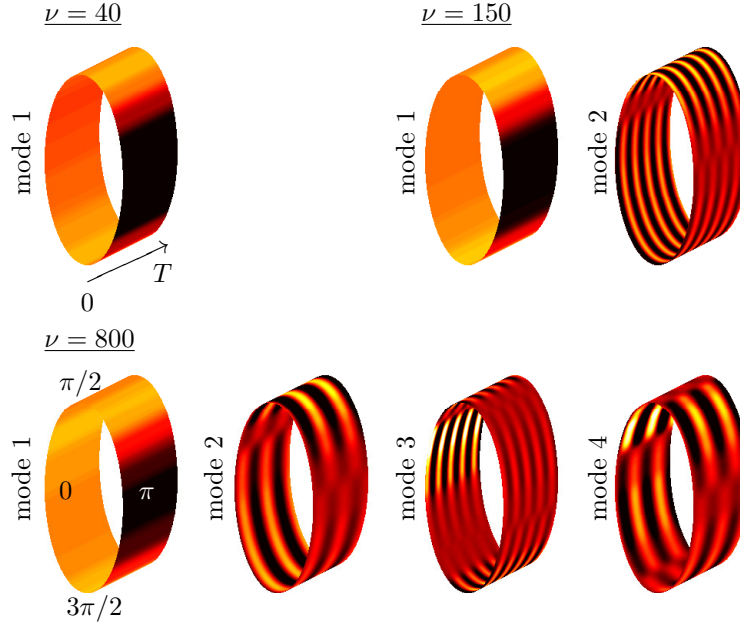


Figure 4: The figure above shows the temporal-spatial modes. These modes corresponds to the specified Reynolds number, and the mode number corresponds to the magnitude of the energy of the specific mode.

6 Conclusion and Outlook

Modern data methods and analysis techniques look to exploit underlying low-dimensional structures in complex data sets. In the case of time-dependent data generated from complex systems, effective methods must capitalize simultaneously on the underlying low-rank structures in both time and space. In doing so, we have demonstrated that one can use a sparse number of spatial sensors that sample randomly (asynchronously) in time to accurately classify the dynamical state of the system even in the presence of noise. The method advocated integrates two transformative tools of analysis: (i) model reduction (machine learning) methods for complex systems and (ii) compressive sensing/sparse representation

The current mathematical architecture and innovation extends previous work on sparse sampling of complex systems by exploiting the nearly periodic time behavior known to be exhibited by many complex systems, including the flow around a cylinder example considered here. Indeed, taking advantage of the sparse signal representation in time allows for better classification of the dynamical state. Moreover it equally, and maximally, exploits the low-dimensional behavior in both time and space. Previous analysis relied on a single measurement in time for performing such classification tasks, thus only exploiting the low-dimensional spatial structures.

The combination of dimensionality reduction and sparsity promoting techniques advocated here can be applied in an exceptionally broad context. Indeed, such algorithmic strategies can be used to enhance computation and efficiently identify measurement locations in a given system by *remembering* the system's key characteristics in both time and space. The low-rank spatio-temporal nature of the approximations used allows construction of control algorithms that wrap around the

dimensionality reduction and sparsity infrastructure—another appealing aspect of the methodology. In conclusion, we advocate a general theoretical framework for complex systems whereby low-rank, spatio-temporal libraries representing the optimal modal basis in time and space are constructed, or learned, from snapshot sampling of the dynamics.

References

- [1] D. Stork P. Hart and R. Duda. *Pattern Classification*. John Wiley & Sons, 2001.
- [2] C. Bishop. *Pattern Recognition and Machine Learning*. Springer, 2007.
- [3] K. Murphy. *Machine Learning: A Probabilistic Perspective*. MIT Press, 2012.
- [4] J. N. Kutz. *Data-Driven Modeling & Scientific Computation: Methods for Complex Systems & Big Data*. Oxford University Press, 2013.
- [5] M. Cross and P. Hohenberg. Pattern formation out of equilibrium. *Reviews of Modern Physics*, 65:851–1112, 1993.
- [6] L.M. Jones, A. Fontanini, B.F. Sadacca, P. Miller, and D.B. Katz. Natural stimuli evoke dynamic sequences of states in sensory cortical ensembles. *Proc. Natl. Acad. Sci. USA*, 104:18772–18777, 2007.
- [7] M. Rabinovich, A. Volkovskii, P. Lecanda, R. Huerta, H.D.I. Abarbanel, and G. Laurent. Dynamical encoding by networks of competing neuron groups: Winnerless competition. *Phys. Rev. Lett.*, 87:068102, 2001.
- [8] M. Rabinovich, R. Huerta, P. Varona, and V.S. Afraimovich. Transient cognitive dynamics, metastability, and decision making. *PLoS Comput. Biol.*, 4:e1000072, 2008.
- [9] G. Laurent, M. Stopfer, R.W. Friedrich, M.I. Rabinovich, A. Volkovskii, and H.D.I. Abarbanel. Odor encoding as an active, dynamical process: Experiments, computation and theory. *Annu. Rev. Neurosci.*, 24:263–297, 2001.
- [10] J.I. Gold and M.N. Shadlen. Representation of a perceptual decision in developing oculomotor commands. *Nature*, 404:390–394, 1999s.
- [11] E. Shlizerman, J. Riffell, and J. N. Kutz. Data-driven modeling of the olfactory neural codes and their dynamics in the insect antennal lobe. (*submitted*), 2013.
- [12] A. Quarteroni and G. Rozza. *Reduced Order Methods for Modeling and Computational Reduction*. Springer, 2013.
- [13] E.J. Candès, J. Romberg, and T. Tao. Robust uncertainty principles: Exact signal reconstruction from highly incomplete frequency information. *Information Theory, IEEE Transactions on*, 52(2):489–509, 2006.
- [14] E.J. Candès, J.K. Romberg, and T. Tao. Stable signal recovery from incomplete and inaccurate measurements. *Communications on pure and applied mathematics*, 59(8):1207–1223, 2006.

- [15] E.J. Candes and T. Tao. Near-optimal signal recovery from random projections: Universal encoding strategies? *Information Theory, IEEE Transactions on*, 52(12):5406–5425, 2006.
- [16] D.L. Donoho. Compressed sensing. *Information Theory, IEEE Transactions on*, 52(4):1289–1306, 2006.
- [17] A. C. Gilbert, J. Y. Park, and M. B. Wakin. Sketched SVD: Recovering spectral features from compressive measurements. *ArXiv e-prints*, 2012.
- [18] R. G. Baraniuk. Compressive sensing. *IEEE Signal Processing Magazine*, 24(4):118–120, 2007.
- [19] R. G. Baraniuk, V. Cevher, M. F. Duarte, and C. Hegde. Model-based compressive sensing. *IEEE Trans. Info. Theory*, 56(4):1982–2001, 2010.
- [20] E. Grossi D. Angelosante, G.B. Giannakis. Compressed sensing of time-varying signals. *16th International Conference on Digital Signal Processing*, 2009.
- [21] I. Bright, G. Lin, and J. N. Kutz. Compressive sensing based machine learning strategy for characterizing the flow around a cylinder with limited pressure measurements. *Physics of Fluids*, 25:127102, 2013.
- [22] S. Brunton, J. Tu, I. Bright, and J. N. Kutz. Compressive sensing and low-rank libraries for classification and reconstruction of nonlinear dynamical systems. *SIAM J. Applied Dynamical Systems*, (submitted), 2013.
- [23] D. Venturi and G.E. Karniadakis. Gappy data and reconstruction procedures for flow past cylinder. *J. Fluid Mech.*, 519:315–336, 2004.
- [24] S. Ganguli and H. Sompolinsky. Compressed sensing, sparsity, and dimensionality in neuronal information processing and data analysis. *Annual Review of Neuroscience*, 35:485–508, 2012.
- [25] B. Olshausen and D. Field. Sparse coding of sensory inputs. *Current Opinion in Neurobiology*, 14:481–487, 2004.
- [26] J.J. Allen and A. J. Smits. Energy harvesting eel. *Journal of Fluid Structures*, 15:629, 2001.
- [27] R Clark and A. J. Smits. Thrust production and wake structure of a batoid-inspired oscillating fin. *Journal of Fluid Mechanics*, 562:415, 2006.
- [28] R. W. Whittlesey, S. C. Liska, and J. O. Dabiri. Fish schooling as a basis for vertical-axis wind turbine farm design. *Bioinspiration and Biomimetics*, 5:035005, 2010.
- [29] J. C. Nawroth, H. Lee, A. W. Feinberg, C. M. Ripplinger, M. L. McCain, A. Grosberg, J. O. Dabiri, and K. K. Parker. A tissue-engineered jellyfish with biomimetic propulsion. *Nature Biotechnology*, 30:792, 2012.
- [30] J. Birch and M. Dickinson. Spanwise flow and the attachment of the leading-edge vortex on insect wings. *Nature*, 412:729, 2001.
- [31] J. O. Dabiri. Optimal vortex formation as a unifying principle in biological propulsion. *Annual Review of Fluid Mechanics*, 41:17, 2009.

- [32] S. P. Sane. The aerodynamics of insect flight. *The Journal of Experimental Biology*, 206:4191, 2003.
- [33] M.J. Shelley and Z. J. Zhang. Flapping and bending bodies interacting with fluid flows. *Annual Review of Fluid Mechanics*, 43:449, 2011.
- [34] Z. J. Wang. Dissecting insect flight. *Annual Review of Fluid Mechanics*, 37:183, 2005.
- [35] T. Y. Wu. Fish swimming and bird/insect flight. *Annual Review of Fluid Mechanics*, 43:25, 2011.
- [36] H. Nyquist. Certain topics in telegraph transmission theory. *American Institute of Electrical Engineers, Transactions of the*, 47(2):617–644, 1928.
- [37] C.E. Shannon. A mathematical theory of communication. *Bell system technical journal*, 27, 1948.
- [38] G. Berkooz, P. Holmes, and J.L. Lumley. The proper orthogonal decomposition in the analysis of turbulent flows. *Annual Rev. Fluid Mech*, pages 539–575, 1993.
- [39] K. Pearson. On lines and planes of closest fit to systems of points in space. *Philosophical Magazine*, 2:559–572, 1901.
- [40] H. Hotelling. Analysis of a complex of statistical variables into principal components. *J. Educ. Psychol.*, 24:417–441, 1933.
- [41] H. Hotelling. Analysis of a complex of statistical variables into principal components. *J. Educ. Psychol.*, 24:498–520, 1933.
- [42] E. N. Lorenz. Empirical orthogonal functions and statistical weather prediction. *Technical report, Massachusetts Institute of Technology*, December, 1956.
- [43] M Gavish and D Donoho. The optimal hard threshold for singular values is $4/3$. (*ArXiv e-prints*), 2014.
- [44] L. N. Trefethen and D. Bau III. *Numerical Linear Algebra*. SIAM, 1997.
- [45] D. Amsallem and C. Farhat. An online method for interpolating linear parametric reduced-order models. *SIAM J. Scientific Comp.*, 33:2169–2198, 2011.
- [46] R Tibshirani. Regression shrinkage and selection via the lasso. *J. Royal. Statist. Soc B.*, 58:267–288, 1996.
- [47] K. Kaspers, L. Mathelin, and H. Abou-Kandil. A statistical learning strategy for flow field estimation from wall-mounted sensors. (*submitted*), 2015.
- [48] K. Kaspers, L. Mathelin, and H. Abou-Kandil. A machine learning approach for constrained sensor placement. (*submitted*), 2015.
- [49] A. E. Deane, I. G. Kevrekidis, G. E. Karniadakis, and S. A. Orszag. Low-dimensional models for complex geometry flows: Application to grooved channels and circular cylinders. *Phys. Fluids*, 3:2337, 1991.

- [50] X. Ma and G. E. Karniadakis. A low-dimensional model for simulating three-dimensional cylinder flow. *J. Fluid Mech.*, 458:181–190, 2002.
- [51] B. Galletti, C. H. Bruneau, and L. Zannetti. Low-order modelling of laminar flow regimes past a confined square cylinder. *J. Fluid Mech.*, 503:161–170, 2004.
- [52] E. Liberge and A. Hamdouni. Reduced order modelling method via proper orthogonal decomposition (pod) for flow around an oscillating cylinder. *J. Fluids Struct.*, 26:292–311, 2010.
- [53] Nektar++: spectral/hp element framework. *www.nektar.info*.